ACS APPLIED MATERIALS & INTERFACES

Research Article

www.acsami.org

Poly(vinylidene fluoride)/NH_2-Treated Graphene Nanodot/Reduced Graphene Oxide Nanocomposites with Enhanced Dielectric Performance for Ultrahigh Energy Density Capacitor

Sunghun Cho,[†] Jun Seop Lee,[†] and Jyongsik Jang*[,†,‡]

[†]Program of Chemical Convergence for Energy and Environment (C2E2), School of Chemical and Biological Engineering, College of Engineering and [‡]School of Chemical and Biological Engineering, College of Engineering, Seoul National University, Shinlimdong 56-1, Seoul 151-742, Korea

Supporting Information

ABSTRACT: This work describes a ternary nanocomposite system, composed of poly(vinylidene fluoride) (PVDF), NH_2-treated graphene nanodots (GNDs), and reduced graphene oxides (RGOs), for use in high energy density capacitor. When the RGO sheets were added to PVDF matrix, the β-phase content of PVDF became higher than that of the pristine PVDF. The surface-treatment of GNDs with an ethylenediamine can promote the hydrogen bonding interactions between the GNDs and PVDF, which promote the formation of β-phase PVDF. This finding could be extended to combine the advantages of both RGO and NH_2-treated GND for developing an effective and reliable means of preparing PVDF/NH_2-treated GND/RGO nanocomposite. Relatively small amounts of NH_2-treated GND/RGO cofillers (10 vol %) could make a great impact on the $\alpha \rightarrow \beta$ phase transformation, dielectric, and ferroelectric properties of the ternary nanocomposite. The resulting PVDF/NH_2-treated GND/RGO nanocomposite exhibited higher dielectric constant ($\varepsilon' \approx 60.6$) and larger energy density ($U_e \approx 14.1$ J cm^{-3}) compared with the pristine PVDF ($\varepsilon' \approx 11.6$ and $U_e \approx 1.8$ J cm^{-3}).

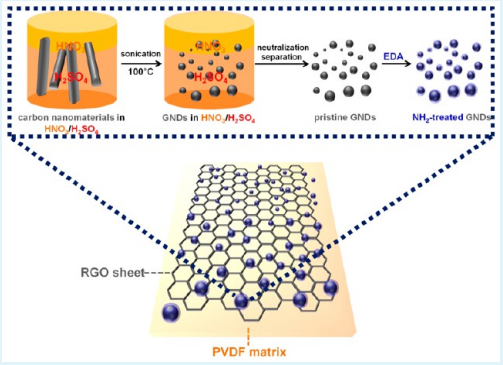

KEYWORDS: *graphene, graphene nanodot, poly(vinylidene fluoride), energy harvester, dielectric capacitor*

INTRODUCTION

Polymer-based nanocomposites have attracted a great deal of interest as high energy density capacitors, since these heterogeneous materials make it possible to combine high dielectric and ferroelectric properties of nanofillers with the high breakdown strength, low dielectric loss, and lightness of polymeric matrices. Among these polymer-based nanocomposites, poly(vinylidene fluoride) (PVDF) is one of the most extensively studied and attractive polymer matrices owing to its fascinating virtues, such as piezoelectric, ferroelectric, and dielectric properties.[1−10] Because of its unique features, PVDF-based nanocomposites have been widely used in a variety of dielectric and ferroelectric devices, such as nonvolatile memories,[11−14] sensors,[15−20] actuators,[19−21] and energy harvesters.[1−8,22−34] The PVDF-based nanocomposites provide an efficient and facile way to obtain high-quality and ferroelectric thin films. In particular, a variety of fillers, such as metal oxides (MO_x),[1−8,16,17,22−27,35,36] conducting polymers (CPs),[18−20,28,30] carbon materials,[21,31−34,37−41] and their mixtures,[19,20,42−46] have been suggested as active phases to significantly improve the intrinsic properties of the PVDF. These active phases induce the growth of β-polymorphs within the PVDF matrices, which provide electroactive properties of the PVDF matrices.[9,10,31,32,35,36] Barium(IV) titanate ($BaTiO_3$)[1−8,22−26,42,43] and lead zirconium titanate (PZT, $Pb(Zr,Ti)O_3$)[1−6,34] are known as the most representative materials for transforming α-phase into β-phase of PVDF crystals because of their significantly higher dielectric constants (each $\varepsilon' \approx 1 \times 10^3$) than the other fillers. Despite their excellent piezoelectric performances, these two materials still suffer from several disadvantages: (1) The dielectric performances of the PVDF containing these two piezoelectric ceramics remains low even after high filler contents are employed; (2) The high filler contents of these two materials usually result in deteriorated flexibility and breakdown strength of the PVDF matrices; (3) Lead-containing materials including PZT usually possess high toxicity, which makes them unsuitable for materials in eco-friendly energy-harvesting devices.[1−8,22−26,34,42,43] Thus, fillers that are more efficient, less brittle, nontoxic, highly flexible, and require smaller filler contents are highly desired for constructing high-performance PVDF-based capacitors.

Graphene, a one-atom-thick planar sheet of sp^2-bonded carbon atoms, is an attractive replacement for the piezoelectric

Received: February 13, 2015
Accepted: April 22, 2015
Published: May 4, 2015

DOI: 10.1021/acsami.5b01430
ACS Appl. Mater. Interfaces 2015, 7, 9668−9681

Scheme 1. Overall Procedure for Fabricating Ternary PVDF/NH_2-Treated GND/RGO Nanocomposite

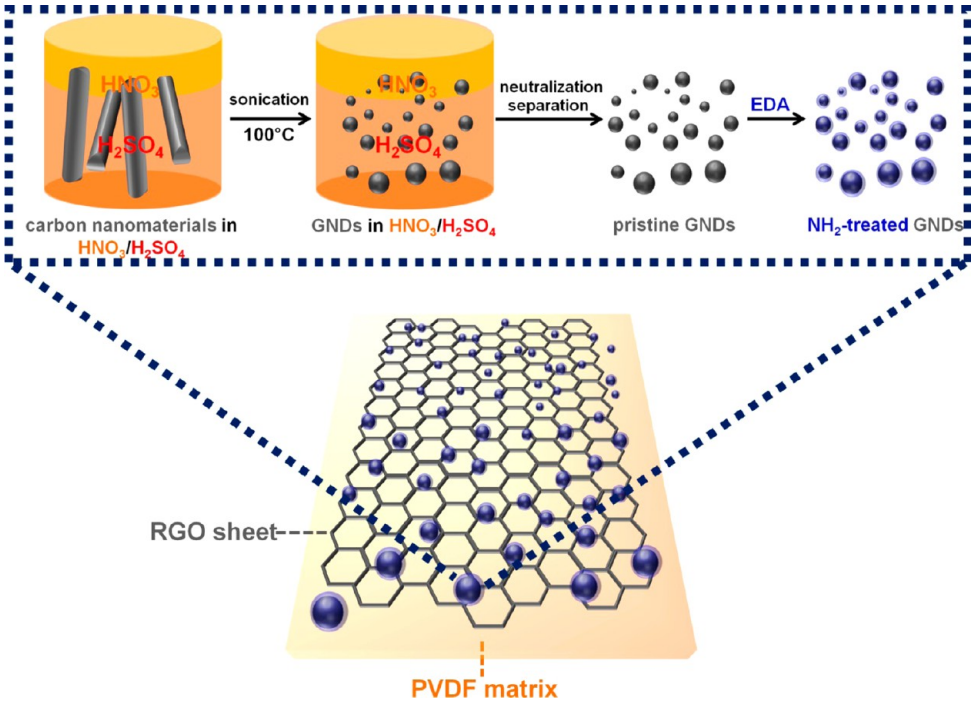

ceramics due to its outstanding electron mobility, thermal stability, mechanical strength, and flexibility.[33,34,37−41,47,48,74−76] Shang et al. incorporated graphene nanosheets (GNS) into the PVDF matrix via an in situ reduction method.[39] Moreover, Achaby et al. reported that the strong molecular interactions between the −C═O groups in GO and the $-CF_2$ in PVDF can also promote the β-phase crystallization of PVDF.[41] Therefore, the increasing graphene content induced more β-phase content of the PVDF crystals, resulting in the enhanced dielectric permittivity and remnant polarization of the graphene-incorporated samples.[33,34,38,39,41] Despite the significant improvements in the dielectric and ferroelectric properties of the graphene-incorporated samples, the PVDF/graphene nanocomposites usually suffer from higher dielectric losses and lower breakdown strength voltages compared with nanocomposites employing the piezoelectric ceramics.[7,8,22−26,34−44] In addition, the graphene sheets behave as defects in the PVDF matrices and tend to deteriorate the breakdown strength of the nanocomposites. This indicates that the volume fractions of the fillers in the PVDF should be reduced to maintain high breakdown electric field and energy density.[21,25] Therefore, the realization of PVDF/graphene nanocomposites having both high dielectric and energy harvesting performances remains a challenge.

Recently, graphene nanodots (GNDs), generally composed of graphene sheets with lateral dimensions less than 100 nm in single-, double-, and few- (3 to 10) layers, are of great interest for developing materials in bioimaging and electronic devices due to their fascinating chemical and physical properties that arise from the quantum-confinement effect.[49−62] In general, the GNDs possess carboxylic acid moieties at the edge, making them suitable for subsequent functionalization with a variety of organic, inorganic, and biological species.[49−62] The surfaces of GNDs have been treated with various functional groups, such as −OH,[49,50,58] −COOH,[59] and $-NH_2$,[60,61] to improve its surface functionality and compatibility with specific atoms or molecules. Moreover, it is well-known that the surface functionality of fillers can significantly promote the formation of the β-phase of the PVDF, which significantly improves the resulting piezoelectric and ferroelectric performances of the nanocomposites.[22−25] Despite the improvements in the synthesis and surface-treatment of the GNDs, the effects of surface-treated GNDs on the phase transformation, dielectric, and ferroelectric properties of the PVDF matrices have seldom been reported. Accordingly, a method for combining the advantages of conventional graphene sheets with the GNDs is highly desired for realizing the high energy density PVDF capacitor device.

Herein, we present a novel and facile method for obtaining PVDF/NH_2-treated GND/reduced graphene oxide (RGO) ternary nanocomposite to develop a high-performance energy harvester. The synergetic effects from RGO sheets and NH_2-treated GNDs on the phase transition, dielectric, and ferroelectric properties of the nanocomposites were systematically investigated. It was found that the RGO sheets having high electroactivity promoted the β-phase formation while disrupting the nucleation of α-phase of the PVDF. Furthermore, the NH_2 groups attached on the surfaces of GNDs effectively interact with the PVDF, thereby offering stronger forces necessary to retain the electroactive phases (β or γ) under thermal energy, while suppressing the α-phase formation. These structural changes of PVDF from α- to β-phase highly affected the resulting dielectric and ferroelectric properties of the nanocomposites. As a result of combining these RGO sheets and NH_2-treated GNDs as cofillers, the ternary nanocomposites exhibited much higher dielectric constants, lower dielectric loss, and larger energy density than the pristine PVDF, PVDF/NH_2-treated GND, and PVDF/RGO nanocomposites.

DOI: 10.1021/acsami.5b01430
ACS Appl. Mater. Interfaces 2015, 7, 9668−9681

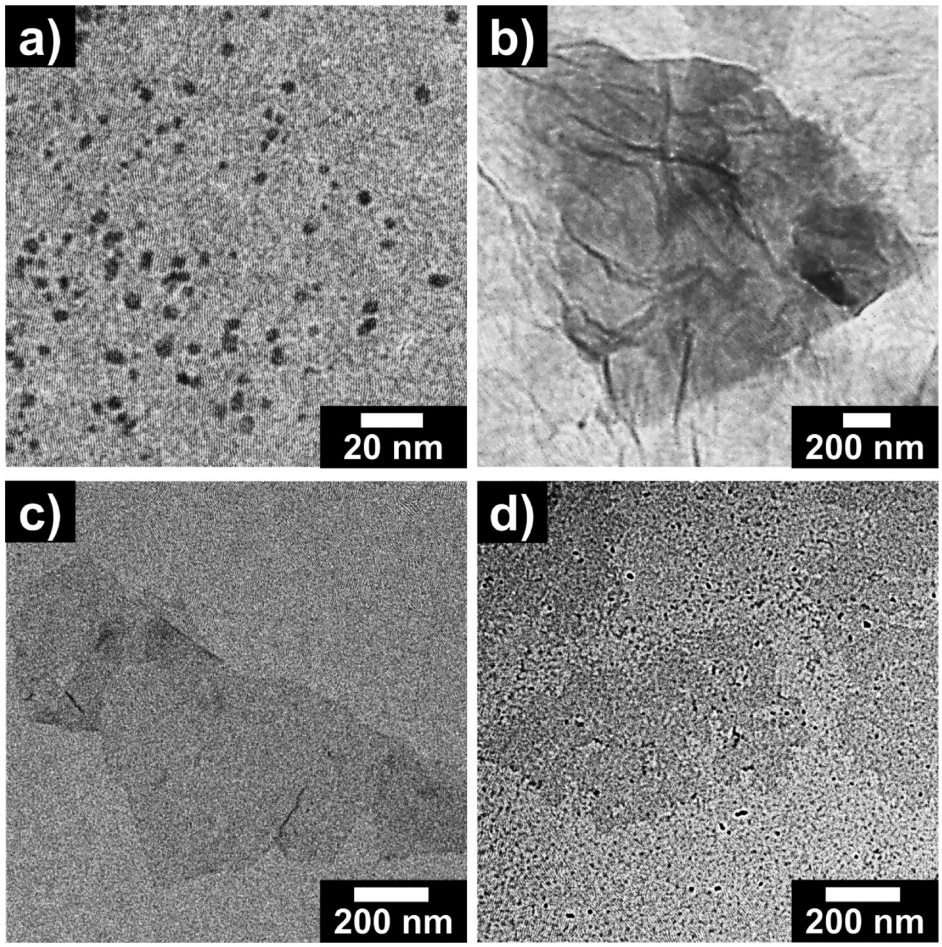

Figure 1. TEM images of (a) NH_2-treated GND, (b) RGO sheet, (c) PVDF/RGO (90:10, v/v), and (d) PVDF/NH_2-treated GND/RGO (90:5:5, v/v/v) nanocomposites. The concentration of fillers in PVDF/RGO and PVDF/NH_2-treated GND/RGO is 10 vol % with respect to PVDF nanocomposites.

■. RESULTS AND DISCUSSION

Fabrication and Characterization of PVDF/NH_2-Treated GND/RGO Nanocomposite. Scheme 1 describes the overall fabrication procedure for PVDF/NH_2-treated GND/RGO nanocomposite. The GNDs were prepared via excessive chemical oxidation of carbon nanofibers (CNFs), since the CNFs can offer facile extraction and size control of the synthesized GNDs.[47−51] To produce the GNDs, the CNFs were added into a mixture of H_2SO_4/HNO_3 (3:1, v/v) followed by neutralization of the excess acid. The neutralized and separated GNDs were treated with ethylenediamine (EDA) to attach the $-NH_2$ groups onto the GNDs, leading to the enhanced hydrogen bonding interaction with the $-CF_2-$ dipoles of the PVDF.[11,12] GO sheets were synthesized according to modified Hummer's method, and the RGO sheets were prepared by the chemical reduction treatment of the GO in a mixture of *N*,*N*-dimethylformamide/water (DMF/water, 95:5, v/v).[47,48,64] Under our experimental condition, the PVDF, RGO, and NH_2-treated GNDs were primarily dispersed in the DMF, DMF/water, and water, respectively. According to Hansen et al., these solvent systems possess similar dispersion (δ_d), hydrogen bonding (δ_h), and polarity interaction (δ_p) parameters (Table S1).[41,63,64] Furthermore, the EDA, a surface modifier of the GNDs, has a similar δ_d value to those of both the water and the DMF. Thus, the stable dispersion of the NH_2-treated GNDs and the RGO sheets could be formed in the DMF/water mixed solvent. Accordingly, both the NH_2-treated GNDs and RGO sheets were highly compatible with the PVDF matrices, which were dispersed in the DMF. As-prepared ternary PVDF/NH_2-treated GND/RGO nanocomposite solution was formed as a highly aligned and uniform thin film via spin-coating method, leading to better distribution of the charged species and enhanced electron transfer within the nanocomposites.[14]

Figure 1a,b represents the transmission electron microscopy (TEM) images of NH_2-treated GND and RGO sheet, which were utilized as cofillers in the PVDF. Average sizes of the NH_2-treated GNDs ranged from ∼3−5 nm, indicating that the cutting processes under the H_2SO_4/HNO_3 mixtures were appropriately performed (Figure 1a).[49−62] The size of RGO sheet used in the present work was ∼1−2 μm, which is similar to that of the graphene sheets obtained from conventional Hummer's method (Figure 1b).[21,47,48,64] To confirm the successful introductions of the NH_2-treated GNDs and RGO sheets to the polymer matrix, TEM images of the PVDF/RGO and the PVDF/NH_2-treated GNDs/RGO nanocomposites are shown in Figure 1c,d, respectively. The size of RGO sheet embedded in the PVDF matrix was similar to that of the TEM image of RGO (Figure 1b,c). Furthermore, it was evident that the NH_2-treated GNDs were highly dispersed throughout the PVDF/RGO surfaces (Figure 1d). These results indicate that

DOI: 10.1021/acsami.5b01430
ACS Appl. Mater. Interfaces 2015, 7, 9668−9681

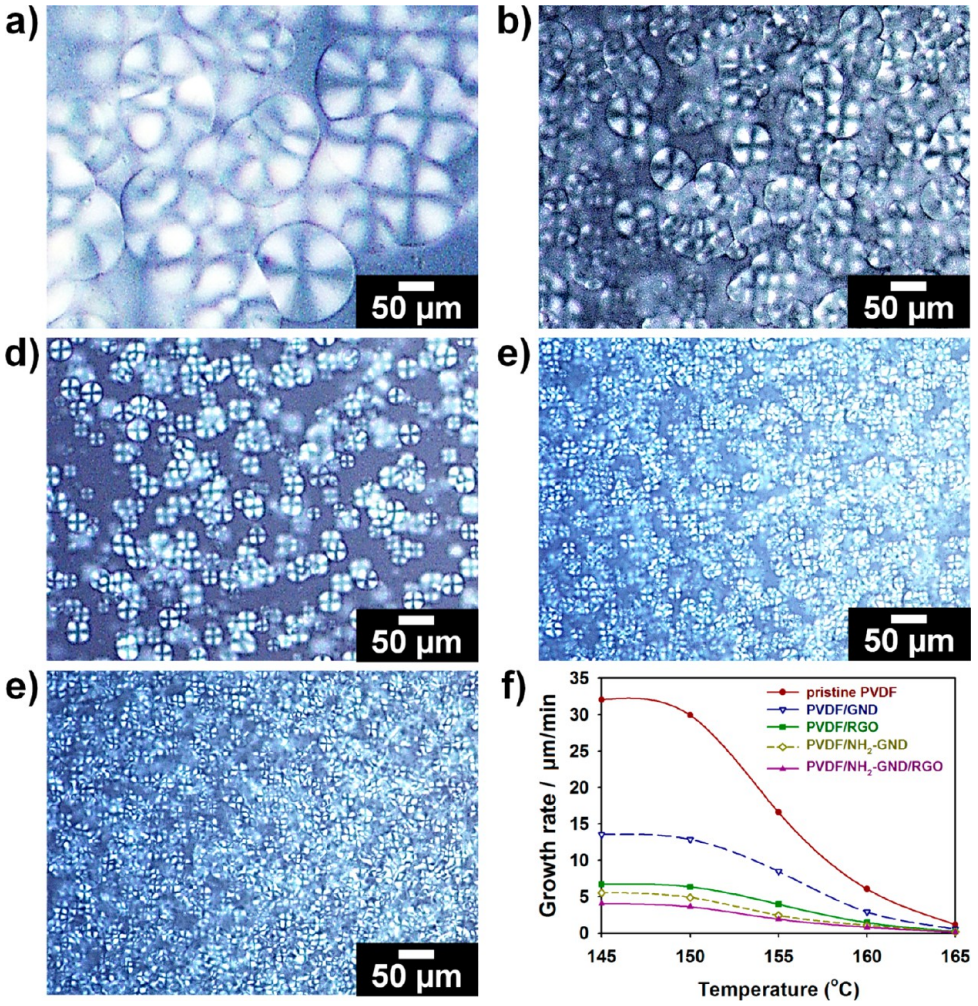

Figure 2. POM images of PVDF nanocomposites containing different fillers after isothermal crystallization at 160 °C: (a) pristine PVDF, (b) GND, (c) RGO, (d) NH_2-treated GND, (e) NH_2-treated GND/RGO. (f) Spherulite growth rate of nanocomposites containing different fillers after isothermal crystallization at 160 °C for 10 min. The concentration of all fillers is 10 vol % with respect to PVDF nanocomposites.

both the GNDs and RGO sheets could be successfully embedded in the PVDF nanocomposite.[47,48]

To observe the effects of NH_2-treated GNDs and RGO sheets on the crystalline behaviors of ternary PVDF/NH_2-treated GNDs/RGO nanocomposite system, the PVDF nanocomposites employing different fillers were isothermally crystallized at 160 °C for 10 min (Figure 2). After the addition of these fillers into the PVDF matrices, the sizes of α-spherulites decreased as follows: PVDF/NH_2-treated GND/RGO < PVDF/NH_2-treated GNDs < PVDF/RGO < PVDF/GND < pristine PVDF (Figure 2a–e, respectively). In addition, the spherulite growth rates of the PVDF nanocomposites, determined as functions of the crystallization temperature and time, exhibited the same tendency as observed in the polarized optical microscopy (POM) images (Figure 2f). Compared with the nanocomposite filled with natural graphite having a size of ~20 μm, the spherulite size and the spherulite growth rate of the PVDF/RGO was slightly higher than that of the PVDF/graphite (Supporting Information, Figure S1). This may be because the fillers with larger sizes can better reduce the chain mobility of the PVDF that is present in the restricted spaces between the fillers.[7] Nevertheless, the PVDF/NH_2-treated GND showed smaller spherulite size and slower spherulite growth rate compared with the PVDF/graphite (Figure S1). This result suggests that the functional groups attached onto the filler surfaces play an important role in interacting with polymer matrix and, thereby, affect the spherulite growth of the PVDF.[22−27] Judging from the results, the movements of the PVDF chains, which mainly cause the dipole losses and β-relaxations of the PVDF, were more effectively restricted by the electroactive RGO sheets than the pristine GNDs, and the $-NH_2$ groups on the GND surfaces provide stronger forces to overcome the thermal energies tending to form the α-phase of the PVDF.[7,22−25,32,33,37]

Raman spectroscopy was performed to confirm the structure of the graphite, GO, RGO, CNF, GND, and NH_2-treated GND (Figure 3a). Two dominant peaks were found in the Raman spectrum of every sample: D band (corresponding to structural defects (1331−1352 cm^{-1})) and G band (related to the vibration of sp^2-hybridized carbon (1572−1608 cm^{-1})).[47,54,78−80] The intensity ratio of the D to the G band (I_D/I_G) ratio of GO was higher than that of the graphite due to the reduced size of the sp^2 domains, which is due to the increase of the disordered structure in the graphene sheets during the extensive oxidation of graphite.[47,78−80] A shift of G peak toward higher wavenumber in the spectrum of GO is attributed to the formation of sp^3 carbon atoms, which resulted from the oxidation of graphite.[47,78−80] After reduction of the

DOI: 10.1021/acsami.5b01430
ACS Appl. Mater. Interfaces 2015, 7, 9668−9681

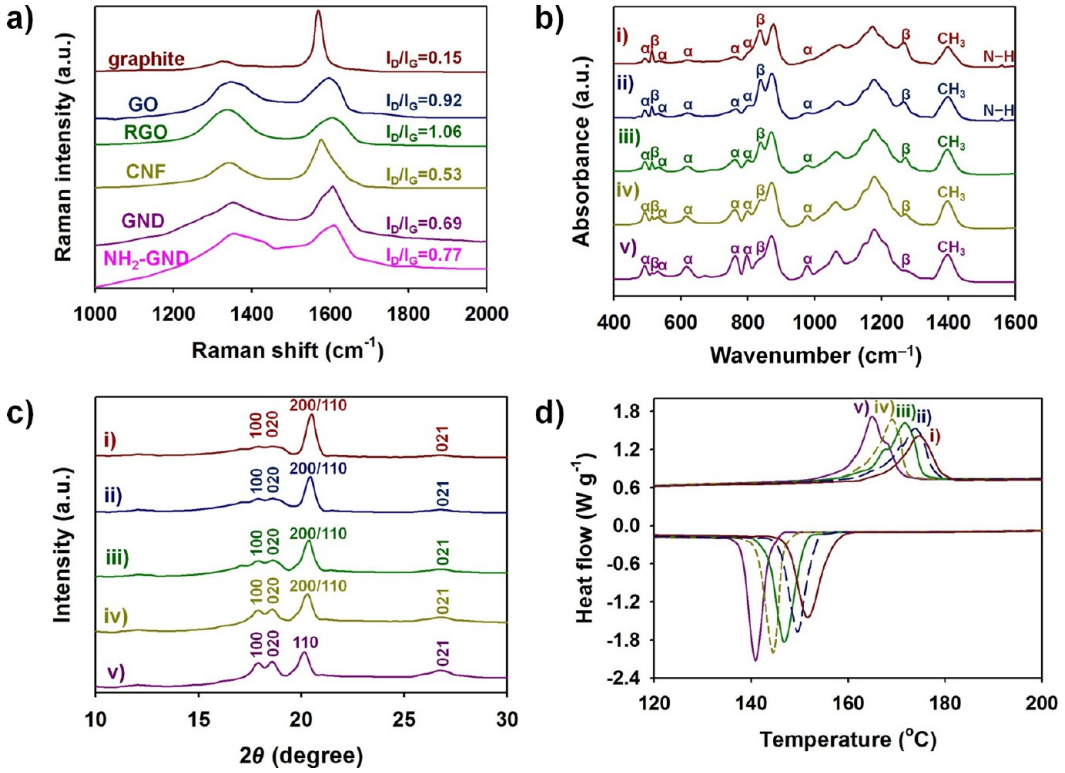

Figure 3. (a) Raman spectra of graphite, GO, RGO, CNF, GND, and NH_2-treated GND. (b) FT-IR spectra, (c) XRD patterns, and (d) DSC thermographs of PVDF nanocomposites filled with NH_2-treated GND/RGO (red), NH_2-treated GND (blue), RGO (green), pristine GND (yellow), and pristine PVDF (purple). The concentration of all fillers is 10 vol % with respect to PVDF nanocomposites.

GO, the I_D/I_G of RGO increased from 0.92 to 1.06, which implies decreased size of the sp^2 domains upon chemical reduction of the GO.[47,73,78−80] In addition, the red shift of the G peak in the RGO may be related to a change in the electronic structure of GO by the hydrazine, which is consistent with the previous work on nitrogen-doped graphene.[47,54,73,78−80] Compared with the CNF, the GND shows a higher I_D/I_G ratio, indicating a reduction in size of the sp^2 domains due to the oxidation in the H_2SO_4/HNO_3 (3:1, v/v) mixture.[47,54] Moreover, the higher I_D/I_G ratio of NH_2-treated GND (0.77) compared with the pristine GND (0.69) indicates a higher degree of defects and disorders of NH_2-treated GND, which may be due to the interaction between the carbon and nitrogen.[78−80] Judging from these results, the reduction of GO sheets and the surface-treatment of GNDs were appropriately carried out.

To confirm the chemical structures of the GO, RGO, pristine GND, and NH_2-treated GND, Fourier-transform infrared (FT-IR) spectra were investigated (Supporting Information, Figure S2a). Several distinctive bands for GO were observed at 1042, 1222, 2382, 1617, and 3440 cm^{-1} in the FT-IR spectrum of the GO (Table S2).[76] The peak intensities for oxygenated functional groups of the GO significantly decreased with the increasing reduction time of the GO from 0.3 to 24 h (Supporting Information, Figure S2b). This indicates that the possibility that hydrogen bonding interaction between the RGO sheets and NH_2-treated GNDs may decrease with the reduction in degree of GO. For this reason, the RGO-1 sample, which had been reduced for 1 h, was chosen as a component for interacting with the NH_2-treated GNDs and PVDF matrix.[41,64−66,76] In the FT-IR spectrum of pristine GNDs, characteristic peaks of GNDs appeared at 835, 1240, 1359, 1594, 1790, 2891, and 2967 cm^{-1} (Supporting Information, Figure S2a and Table S3).[49−59,76] After the GNDs were treated by $-NH_2$ groups, the peaks for $-NH_2$, N−H, and C−N bonds were intensified compared to those for the pristine GNDs, and these peaks originated from the EDA, which is a water-soluble and difunctional amine. Therefore, the amine-functionalization of the GNDs could be successfully conducted in water by using the EDA.[60−62,76] FT-IR spectra of the PVDF nanocomposites employing different fillers were investigated to observe the effects of the NH_2-treated GNDs and RGO sheets on the chemical structures and phase transitions of the PVDF matrices (Figure 3b and Table S4). Several absorption bands at 615, 764, 796, and 978 cm^{-1} are ascribed to the α-phase of the PVDF, and the absorption bands for the β-phase appeared at 839 and 1273 cm^{-1} (Table S4).[7,8,32,76,77] After the addition of fillers, the peaks assigned to the β-phase became significantly stronger and sharper, while the peaks corresponding to the α-phase became indistinctive. More specifically, the relative intensity ratio of β-phase in the FT-IR spectra was estimated using eq 1:

$$\frac{I_\beta}{I_\alpha + I_\beta} = \frac{I_{513} + I_{839} + I_{1272}}{I_{491} + I_{530} + I_{615} + I_{764} + I_{796} + I_{978} + I_{513} + I_{839} + I_{1272}} \quad (1)$$

where the I_α and I_β denote the peak intensity for α and β-phases, respectively. I_{491}, I_{513}, I_{530}, I_{615}, I_{764}, I_{796}, I_{839}, I_{978}, and I_{1272} indicate the peak intensity of absorption bands at 491, 515, 530, 615, 764, 796, 839, 978, and 1272 cm^{-1}, respectively. Because of the extremely infinitesimal amounts of the peaks for γ-phase phase (779, 813, and 1234 cm) in Figure 3b, the presence of γ-phase was neglected in eq 1. The relative proportion of β-phase in the FT-IR spectra increased as follows: pristine PVDF (0.29) < PVDF/pristine GND (0.44) <

DOI: 10.1021/acsami.5b01430
ACS Appl. Mater. Interfaces 2015, 7, 9668−9681

PVDF/RGO (0.59) < PVDF/NH_2-treated GND (0.69) < PVDF/NH_2-treated GND/RGO (0.78). It was evident that the proportion of β-phase increased after the addition of NH_2-GNDs and RGO into the PVDF. The enhanced formation of the β-phase over the α-phase was strongly associated with the synergetic effects from the NH_2-treated GNDs and RGO sheets.[37−40]

To identify the effects of the prepared fillers on the crystalline phase structure of PVDF nanocomposites, the XRD patterns of the NH_2-treated GNDs, RGO sheets, and PVDF nanocomposites containing different fillers are shown in Figure 3c. In the XRD pattern of the NH_2-treated GNDs, a broad peak at 2θ = 20.3° with an interlayer distance of 4.38 Å was found, while the RGO sheets exhibited a broad peak at 2θ = 24.5° (3.63 Å; Supporting Information, Figure S3). The interlayer distances of these two samples were close to that of the graphite (3.39 Å), indicating that these two material were originated by the carbons.[37−41,47−65] In the XRD spectra of the PVDF nanocomposites, the characteristic peaks of α-phase, corresponding to the (100), (020), (110), and (021) planes, appeared at 2θ = 17.7°, 18.6°, 20.1°, and 26.5°, and the diffraction peak of β-phase, relating to the (200)/(110) plane, was observed at 2θ = 20.4−20.6° (Figure 3c). To estimate the relative proportion of the XRD peaks for β-phase, the relative ratio of the peak intensities for (200/110), (100), (020), (110), and (021) was estimated as follows:

$$\frac{I_\beta}{I_\alpha + I_\beta} = \frac{I_{200/110}}{(I_{100} + I_{020} + I_{110} + I_{021})_\alpha + (I_{200/110})_\beta} \quad (2)$$

where the I_{100}, I_{020}, I_{110}, I_{021}, and $I_{200/110}$ mean the peak intensity at (100), (020), (110), (021), and (200/110) planes, respectively. Because of the absence of a peak for (200)/(110) in the XRD pattern of pristine PVDF, eq 2 was utilized to determine the crystalline state of the nanocomposites containing the GND, RGO, and NH_2-treated GND. Obviously, the relative proportion of β-phase in the XRD patterns increased in the following order: PVDF/GND (0.51) < PVDF/RGO (0.53) < PVDF/NH_2-treated GND (0.57) < PVDF/NH_2-treated GND/RGO (0.64) (Table 2). The calculated values were in good agreement with the values obtained from the FT-IR analysis. In addition, the β-phase peak shifted to a higher angle after the addition of fillers: pristine PVDF (20.4) ≈ PVDF/GND (20.4) < PVDF/RGO (20.5) ≈ PVDF/NH_2-treated GND (20.6). No significant changes were found in the XRD spectrum after the addition of pristine GNDs, while the NH_2-treated GNDs and RGO sheets resulted in significant decreases in the α-polymorphs and much greater increases in the β-polymorph of the PVDF. These results suggest that these two different filler systems played an important role in inducing the β-phase crystals, thereby retarding the crystallization of α-phase of PVDF.[7−10,37−41,67,68] Judging from these results, the enhanced β-phase formation of the ternary nanocomposites was mainly attributable to the synergetic effects from the advantage of each component: (1) NH_2-treated GNDs provide stronger dipole−dipole forces and hydrogen bonding interactions with the PVDF matrices; (2) Higher aspect ratios and electroactive properties of the RGO sheets effectively restricted the molecular movements of the PVDF chains.[22−25,32,37−41,60−62] To further analyze the crystallization behaviors of the PVDF nanocomposites, the differential scanning calorimetry (DSC) thermographs of the PVDF/GSs nanocomposites are shown in Figure 3d and Table 1. After addition of the GND, RGO, NH_2-treated GND, and NH_2-treated GND/RGO into the PVDF matrices, the melting temperature (T_m) increased by 4.3, 6.5, 8.4, and 9.3 °C, respectively, relative to the pristine PVDF. During the cooling processes of the samples, the nanocomposites employing the GND, RGO, NH_2-treated GND, and NH_2-treated GND/RGO crystallized at 4.8, 6.1, 8.1, and 11.3 °C higher temperatures, respectively, with respect to the pristine PVDF. Furthermore, the equilibrium melting point (T_m^0) of the samples was determined using the Hoffman−Weeks eq 3

Table 1. Differential Scanning Calorimetry Data of PVDF Nanocomposites with Different Fillers

sample[a]	T_m (°C)	T_c (°C)	x^b	y^c	ΔH_m (J g^{-1})	X_c (%)[d]
pristine PVDF	164.9	140.9	0.68	0.32	45.2	46.9
PVDF/GND	169.1	144.5	0.58	0.42	44.1	45.3
PVDF/RGO	171.6	146.6	0.35	0.65	42.5	42.6
PVDF/NH_2-GND	173.9	149.4	0.29	0.71	40.2	40.1
PVDF/NH_2-GND/RGO	175.3	151.4	0.19	0.81	37.0	36.5

[a]The concentration of all fillers is 10 vol% with respect to PVDF nanocomposites. [b]Weight fraction of α-phase was estimated from the peak intensity of multiple melting peaks at higher temperature. [c]Weight fraction of β-phase was estimated from the peak intensity of multiple melting peaks at lower temperature. [d]The value was calculated using eq 4.

$$T_m = \eta T_c + (1 - \eta) T_m^0 \quad (3)$$

where T_m, T_c, and T_m^0 are melting point, crystalline temperature, and equilibrium melting point of the sample, respectively. A value of η = 0 reflects the perfectly stable crystals, while a value of η = 1 implies that the crystals are inherently unstable.[81,82] Compared with that of the pristine PVDF, the η of PVDF/NH_2-treated GND/RGO nanocomposite increased from 0.32 to 0.38, which may be due to the presence of crystalline defects in the PVDF nanocomposite.[81,82] The value of T_m^0 (°C) of the samples increased as follows: pristine PVDF (176.2) < PVDF/GND (182.3) < PVDF/RGO (185.1) < PVDF/NH_2-treated GND (188.2) < PVDF/NH_2-treated GND/RGO (189.9) (Supporting Information, Figure S4 and Table S5). These results indicate that the RGO sheets and NH_2-treated GNDs acted as nucleating agents for improving the thermal stability of PVDF nanocomposites.[7,8,42,67,68] More specifically, two multiple melting peaks were found in the DSC thermographs for the nanocomposites. These multiple melting peaks are may be due to the coexistence of α to β-phases in the PVDF nanocomposites, as discussed in Figure 3b. The peak at lower temperature is associated with the α-phase, while the peak at higher temperature indicates the β-phase. The degree of crystallinity (X_c) of the PVDF nanocomposites was calculated using eq 4:

$$X_c = \frac{\Delta H_m}{x\Delta H_\alpha + y\Delta H_\beta} \times 100\% \quad (4)$$

where the ΔH_m, ΔH_α, and ΔH_β refer to the heat of fusions of sample, 100% crystalline α-PVDF (93.0 J g^{-1}), and β-PVDF (103.4 J g^{-1}), respectively.[7,42,67,68] The x and y denote the weight fraction of the α- and β-phases in the sample, respectively. It was observed that the x value decreased, while

DOI: 10.1021/acsami.5b01430
ACS Appl. Mater. Interfaces 2015, 7, 9668−9681

the y value increased after the addition of the fillers. Although there was slight difference between the proportion values of β-phase estimated from the FT-IR, XRD, and DSC data, clearly the tendency observed in the DSC thermographs was in good accordance with those of the FT-IR and DSC analyses (Table 2). Therefore, the ΔH_m and X_c values decreased after the addition of fillers, which confirms that the presences of the NH_2-treated GNDs and RGO sheets can significantly reduce the contents of the α-phase in the samples by obstructing the movement of polymer chains of the α-PVDF. Considering these results, the NH_2-treated GND/RGO cofiller system efficiently promotes the dipole polarizations and hydrogen bonding interactions, which consequently increase the β-phase crystals of the PVDF.[7,42,67,68]

Table 2. Relative Proportion of β-Phase in the Pristine PVDF and the Nanocomposites Filled with Different Fillers Obtained from the FT-IR, XRD, and DSC Measurements

sample[a]	FT-IR[b]	XRD[c]	DSC[d]
pristine PVDF	0.29		0.19
PVDF/GND	0.44	0.51	0.29
PVDF/RGO	0.59	0.53	0.35
PVDF/NH_2-GND	0.69	0.57	0.58
PVDF/NH_2-GND/RGO	0.78	0.64	0.68

[a]The concentration of all fillers is 10 vol% with respect to PVDF nanocomposites. [b]The value was calculated using eq 1. [c]The value was calculated using eq 2. [d]The value was estimated from the multiple melting peaks.

To confirm the effects of annealing temperatures on the formation of γ-phase in the PVDF nanocomposites, the samples were crystallized at 160 °C for 24 h after being annealed at 170 or 180 °C and quickly cooled (30 °C min^{-1}) to room temperature (Figure 4). In the POM images of the annealed samples, it was evident that the sizes of spherulites annealed at 180 °C were smaller than those of samples annealed at 170 °C. The ringed spherulites of PVDF may be the mixture of α- and γ-phase, and the different spherulite sizes may be due to the different proportion of each phase in the spherulites.[83,84] According to Prest and Luca, the rate of the α- to γ-phase transformation increases with temperature and heating time.[85] In the FT-IR spectra of the samples annealed at 180 °C, the peaks for γ-phase appeared at 779, 813, and 1234 cm^{-1} in the FT-IR spectra of every sample (Supporting Information, Figure S5 and Table S4).[76,77] Thus, the decreased spherulites of the annealed samples may be related to the increase in the formation of γ-phase. The spherulite sizes of samples decreased as follows: PVDF/NH_2-treated GND/RGO < PVDF/NH_2-treated GND < PVDF/RGO < PVDF/GND < pristine PVDF. To confirm the relationship between the spherulite size and the content of γ-phase, the relative intensity ratio of γ-phase in the FT-IR spectra was estimated using eq 5:

$$\frac{I_\gamma}{I_\alpha + I_\beta + I_\gamma} = (I_{779} + I_{813} + I_{1234})/(I_{491} + I_{530} + I_{615} + I_{764} + I_{796} + I_{978} + I_{513} + I_{839} + I_{1272} + I_{779} + I_{813} + I_{1234}) \quad (5)$$

where I_γ refers to the peak intensity for γ-phase. I_{779}, I_{813}, and I_{1234} indicate the peak intensity of absorption bands at 779, 813, and 1234 cm^{-1}, respectively. The relative proportion of γ-phase in the FT-IR spectra increased as follows: pristine PVDF (0.17) < PVDF/pristine GND (0.22) < PVDF/RGO (0.26) < PVDF/NH_2-treated GND (0.28) < PVDF/NH_2-treated GND/RGO (0.30) (Supporting Information, Figure S5 and Table S4). However, the relative proportions of the γ-phase estimated from the FT-IR spectra were not high as expected in the POM image, since the peak intensity around 839 cm^{-1}, which may be overlapped with the peak for γ-phase (833−835 cm^{-1}), was not considered as a component for γ-phase in the calculation.[76,77] Nevertheless, the peaks for γ-phase increased with decreasing spherulite sizes of the annealed samples, as shown in the POM images. It is considered that these fillers play an important role in obstructing the thermodynamically stable α-PVDF at higher temperature, and, thereby, the formation of polar γ-phase could be promoted.[7]

To study the static light-scattering of the PVDF/NH_2-treated GND/RGO nanocomposite, the vertically polarized incident light (V_v) and horizontally polarized incident light (H_v) scattering profiles of the nanocomposite solutions for different contents of the PVDF/NH_2-treated GND/RGO (1, 2, 5, and 10 wt %) are represented in Figure 5. Figure 5a represents the V_v scattering profiles of the samples. The intensities of the V_v peaks decreased with increasing content of the PVDF/NH_2-treated GND/RGO, while the positions of the V_v peaks shifted toward the larger scattering vector (q). The results may be due to the amplitude and the shape of the V_v peaks being highly dependent on the PVDF content.[86−88] The H_v scattering profiles of the nanocomposite solutions for the 1, 2, 5, and 10 wt % PVDF/NH_2-treated GND/RGO nanocomposites are shown in Figure 5b. A shift of H_v peaks toward the larger q may be due to the increase in the PVDF/NH_2-treated GND/RGO content, and the results were in good agreement with the V_v scattering profiles. However, in contrast to the V_v scattering results, the magnitudes of the H_v peaks increased with the increasing PVDF/NH_2-treated GND/RGO content.[86−88] Considering these results, both the V_v and H_v scattering behaviors of the nanocomposite solutions were highly affected by the content of PVDF/NH_2-treated GND/RGO.

Dielectric and Energy-Harvesting Performances of PVDF/NH_2-Treated GND/RGO Nanocomposite. The frequency dependencies of the dielectric constant (ε') and dielectric loss (ε'') of the nanocomposites employing the GND, RGO, NH_2-treated GND, and NH_2-treated GND/RGO cofiller are shown in Figure 6. The ε' of the nanocomposites containing different fillers increased in the following order: NH_2-treated GND/RGO (60.6) > NH_2-treated GND (35.0) > RGO (21.9) > GND (15.2) > pristine PVDF (11.6), at a frequency of 1×10^2 Hz (Figure 6a). According to mathematical expressions of the dielectric behaviors proposed by Bhimasankaram et al.[69] and Furukawa et al.,[70] the dielectric constant of the nanocomposites is mainly dependent on the dielectric constants of pristine PVDF (ε_1) and fillers (ε_2) and the volume fraction of fillers (q). However, neither theoretical model considers the interfacial interactions between the polymer matrices and fillers. The large enhancement in the dielectric constant of the PVDF/NH_2-treated GND/RGO nanocomposite can be attributed to the Maxwell−Wagner−Sillars interfacial polarization because of the different conductivity and interfacial interactions between the PVDF, RGO sheets, and NH_2-treated GNDs.[7,8,37,38] Furthermore, the dielectric loss, $\varepsilon''/\varepsilon' = \tan\delta$, decreased in the order of NH_2-treated GND/RGO (0.041) < NH_2-treated GND (0.055) < RGO (0.064) < GND (0.080) < pristine PVDF (0.084), at a frequency of 1×10^3 Hz (Figure 6b). The dielectric loss of nanocomposites mainly resulted from the α-phase contents in the PVDF matrices, whereas the fillers played an important role

DOI: 10.1021/acsami.5b01430
ACS Appl. Mater. Interfaces 2015, 7, 9668−9681

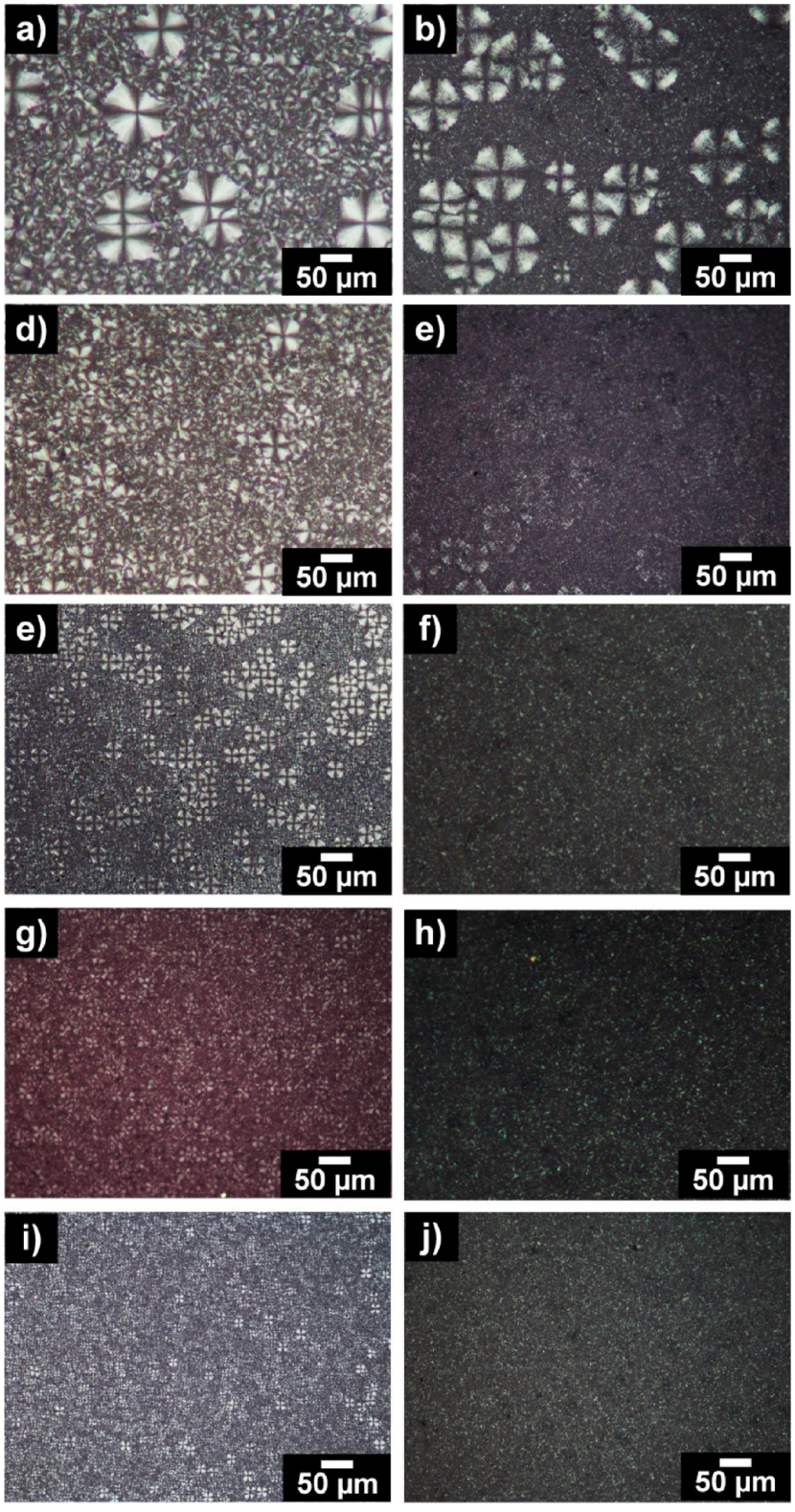

Figure 4. POM images of pristine PVDF (a, b) and PVDF nanocomposites containing GND (c, d), RGO (e, f), NH_2-treated GND (g, h), and NH_2-treated GND/RGO (i, j) after isothermal crystallization at 160 °C for 12 h after being heated at 170 °C (a, c, e, g, i) or 180 °C (b, d, f, h, j) and cooled to room temperature. The concentration of all fillers is 10 vol % with respect to PVDF nanocomposites.

in reducing the α-phase contents of the PVDF.[7,22−25,43,44] This indicates that the NH_2-treated GNDs and RGO sheets disrupt the movements of the molecular chains of PVDF, which results in the decreases of the dipole loss and β-relaxation.[7,8,43,44] Accordingly, the decrease in dielectric loss of the PVDF nanocomposites filled with GNDs and RGO sheets may be due to the minimized dipole losses and β-relaxation. Consequently, the synergetic effects from the surface functionality on the GND surfaces and high electroactivity of the RGO further

DOI: 10.1021/acsami.5b01430
ACS Appl. Mater. Interfaces 2015, 7, 9668−9681

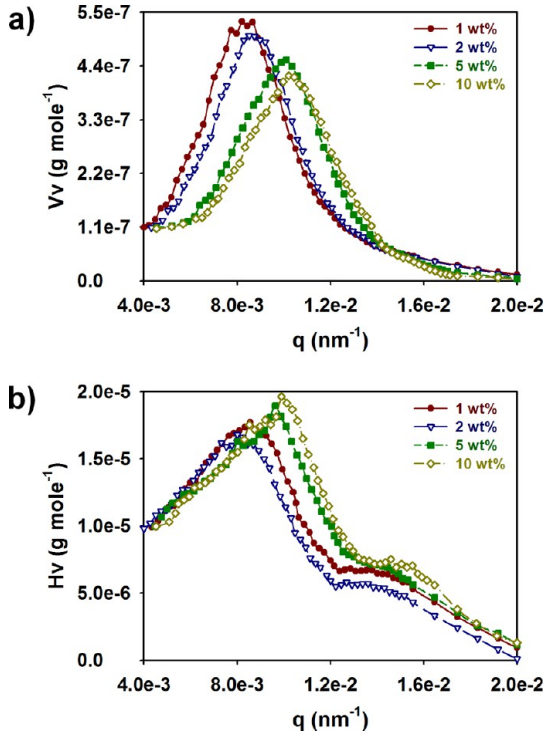

Figure 5. Normalized (a) V_v and (b) H_v scattering intensity profiles of PVDF/NH_2-treated GND/RGO nanocomposite soultions measured at 45 °C for different PVDF/NH_2-treated GND/RGO contents (1, 2, 5, and 10 wt %). The concentration of all fillers is 10 vol % with respect to PVDF nanocomposites.

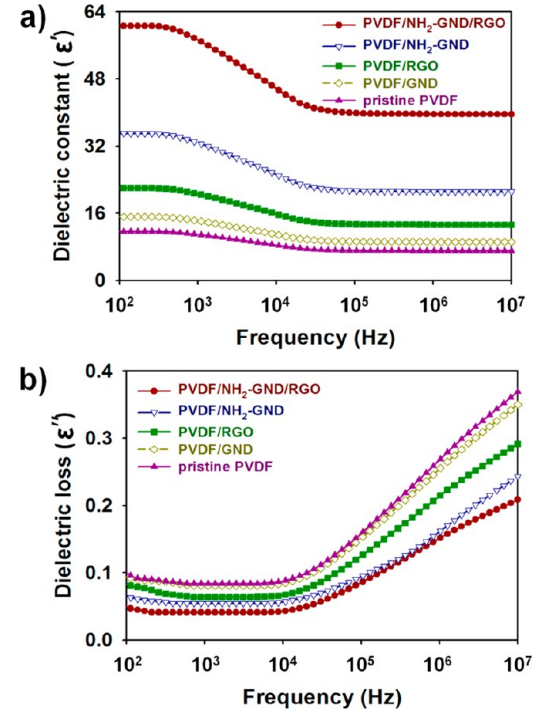

Figure 6. Dependences of (a) dielectric constants and (b) dielectric losses of PVDF nanocomposites with different fillers on frequency from 1 × 10^2 to 1 × 10^7 Hz, respectively. The concentration of all fillers is 10 vol % with respect to PVDF nanocomposites.

enhanced the resulting dielectric constant of the ternary PVDF/NH_2-treated GND/RGO nanocomposite system.

According to previous work on the dielectric capacitors, the energy density of the linear dielectric capacitors can be expressed as $\kappa_{eff}\varepsilon_0 E_b^2/2$, where κ_{eff}, E_b, and ε_0 denote the effective permittivity of the film, breakdown strength, and vacuum permittivity (8.85 × 10^{-12} nF m^{-1}).[22−34] As energy-harvesting behaviors of most ferroelectric materials are not linearly dependent on the applied electric fields, the energy densities of the nanocomposites were estimated from the *P*−*E* curves (Figure 7)[22−34,71,72] according to the equation U_e = $\int E dD$, where *E* and *D* denote the electric field and dielectric displacement of the nanocomposite, respectively. After the addition of the fillers, the energy density of the samples increased in the following order (J cm^{-3}): pristine PVDF (1.8) < GND (3.4) < RGO (5.2) < NH_2-treated GND (7.9) < NH_2-treated GND/RGO (14.1). Moreover, the breakdown strength electric field of the nanocomposites employing GND, RGO, NH_2-treated GND, and NH_2-treated GND/RGO were measured as 3.75 × 10^3, 3.84 × 10^3, 3.92 × 10^3, and 3.90 × 10^3 kV cm^{-1}, respectively, and these values were almost identical to that of the pristine PVDF (3.99 × 10^3 kV cm^{-1}). The small decreases and high retentions in the breakdown strengths of the nanocomposites can be explained by the following points: (1) The NH_2 groups attached onto the GND surfaces could enhance the compatibility with the PVDF matrix by hydrogen bonding interactions, which prevent the propagation of defects through the interfaces between the GNDs and PVDF matrix ; (2) Higher aspect ratios of the RGO sheets than those of the GNDs may promote the in-plane orientation of the nanocomposites.[22−34] Combined with the results of the dielectric properties discussed above, the ternary PVDF/NH_2-treated GND/RGO nanocomposite benefits from the synergistic effects of the enhanced compatibility and dipole polarizations at the PVDF/GND interfaces due to the NH_2−treated GNDs, combined with the highly electroactive RGO sheets.

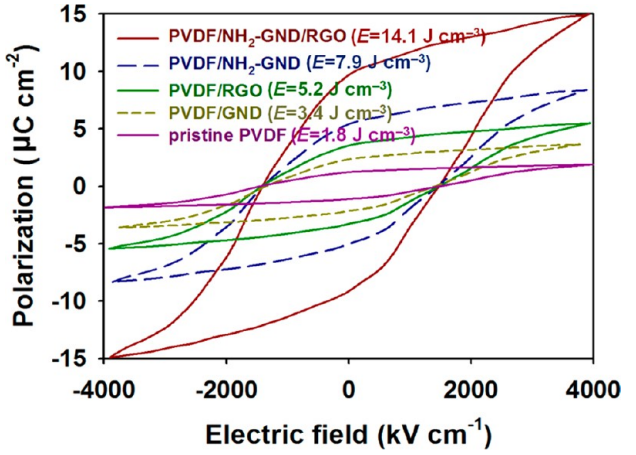

Figure 7. Hysteresis loops of polarization−electric field (*P*−*E*) curves of PVDF nanocomposites with different fillers on frequency from 1 × 10^2 to 1 × 10^7 Hz, respectively. The concentration of all fillers is 10 vol % with respect to PVDF nanocomposites.

To evaluate the practical applicability of the ternary PVDF/NH_2-treated GND/RGO nanocomposite system as an energy-harvesting device, overall performances of this work and the other state-of-art work are summarized in Figure 8.[27,45,46] Compared with the other work, the ternary PVDF/NH_2-treated GND/RGO nanocomposite system has shown

DOI: 10.1021/acsami.5b01430
ACS Appl. Mater. Interfaces 2015, 7, 9668−9681

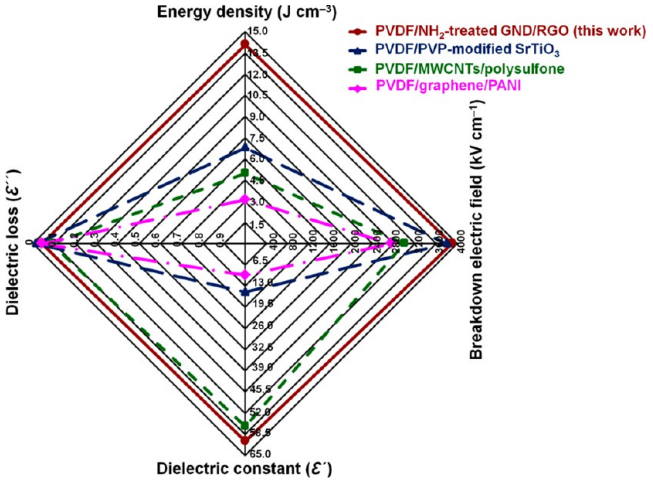

Figure 8. Radar plots comparing this work and state-of-art work cited from refs 27, 45, and 46.

enhanced dielectric constant, energy density, and breakdown strength. Judging from these facts, the ternary PVDF/NH_2-treated GND/RGO nanocomposite has a great potential as an energy-harvesting device.

■. CONCLUSIONS

A facile and effective strategy for enhanced dielectric and energy-harvesting performances has been demonstrated by the ternary PVDF/NH_2-treated GND/RGO nanocomposite system. NH_2-treated GNDs were readily synthesized by excessive chemical oxidation of CNFs followed by surface treatment using the EDA, and these NH_2-treated GNDs were highly compatible with the RGO sheets and PVDF matrix. The NH_2-treated GND/RGO dual cofillers provided the effective dipole polarizations and the nucleation of β-phase crystals of the PVDF in the nanocomposites due to the enhanced dipole−dipole forces, hydrogen-bonding interactions, and improved compatibility with the PVDF matrix. Furthermore, such enhancement in the β-phase formation of the PVDF/NH_2-treated GND/RGO nanocomposite directly affected its dielectric and energy-harvesting performances. The nanocomposite employing the NH_2-treated GND/RGO dual cofillers has shown significantly improved dielectric ($\varepsilon' \approx 60.6$) and energy-harvesting performances ($U_e \approx 14.1$ J cm^{-3}) compared with the pristine PVDF ($\varepsilon' \approx 11.6$ and $U_e \approx 1.8$ J cm^{-3}) and nanocomposites containing NH_2-treated GNSs ($\varepsilon' \approx 35.0$ and $U_e \approx 7.9$ J cm^{-3}), RGO sheets ($\varepsilon' \approx 21.9$ and $U_e \approx 5.2$ J cm^{-3}), and GNDs ($\varepsilon' \approx 15.2$ and $U_e \approx 3.4$ J cm^{-3}). The procedure described herein can be useful for combining graphene-based materials efficiently with the polymer matrices to realize high-performance actuator, sensor, and energy-harvesting devices.

■. EXPERIMENTAL SECTION

Materials. Polyvinylidene fluoride (PVDF, molecular weight ca. 275 000 by GPC), ethylenediamine (EDA, 99%), natural flake graphite, sodium carbonate (Na_2CO_3, 99.5%), sodium nitrate ($NaNO_3$, 99%), hydrazine monohydrate ($N_2H_4{\cdot}H_2O$, 98%), *N*,*N*-dimethylformamide (DMF, 99.8%), nitric acid (HNO_3, 70%), and absolute ethanol were purchased from Sigma-Aldrich (St. Louis, MO). Carbon nanofibers (CNFs; NEXCARB-H, <50 nm) was obtained from Suntel Co. (Korea). Potassium permanganate ($KMnO_4$, 99.3%) and phosphorus pentoxide (P_2O_5, extra pure) were obtained from Junsei Chemical Co. (Tokyo, Japan). Potassium persulfate ($K_2S_2O_8$, 99%) was purchased from Kanto Chemical Co. (Tokyo, Japan). Sulfuric acid (H_2SO_4, 95%), sodium hydroxide (NaOH, 99%), hydrogen peroxide (H_2O_2, 30−35.5%), and hydrochloric acid (HCl, 35−37%) were purchased from Samchun (Seoul, Korea).

Synthesis of Pristine Graphene Nanodots. NH_2-treated GNDs were synthesized using the modified top-down approach method. In detail, 0.40 g of CNFs were introduced into a mixture of concentrated 90 mL of H_2SO_4 and 30 mL of HNO_3. The mixture solution was sonochemically treated for 2 h at 100 °C followed by vigorous stirring for 1 d. As-prepared mixture was cooled and diluted with 800 mL of distilled water. The pH of the GND solution containing the cut CNFs was neutralized to 8 using Na_2CO_3, after which the aqueous solution of GNDs was obtained.

Separation of GNDs. The separation of the aqueous solution of GNDs was conducted to obtain the isolated GNDs. In the first step, the solution of GNDs was diluted to one-fifth of its initial volume followed by addition of absolute ethanol to the diluted solution in a volume ratio of 2:1. To separate the precipitates from the supernatants in the turbid solution, it was centrifugated at 15 000 rpm for 30 min. The supernatant (supernatant/absolute ethanol = 1:2 by volume) obtained from the procedure discussed above was dispersed in the absolute ethanol. The diluted supernatant solution was centrifugated at 15 000 rpm for 30 min, resulting in another fraction of supernatant and precipitate. These processes discussed above were repeatedly conducted three times to obtain fractions of GNDs having a uniform size.

Collection of Pristine Graphene Nanodots. The supernatant solution of GNDs was heated at 120 °C for 1 h in an autoclave and then cooled to room temperature. The dried GNDs (30 mg mL^{-1} in water, 3.0 wt % with respect to water) were redispersed in distilled water using sonochemical treatment for 1 h, and the redispersed aqueous solution of GNDs was used as fillers in the nanocomposite.

Surface Treatement and Collection of NH_2-Treated Graphene Nanodots. The supernatant solution of GNDs was treated with 2 mL of ethylenediamine (EDA) to functionalize the surfaces of GNDs. The mixture solution contating EDA was heated at 120 °C for 1 h in an autoclave and then cooled to 25 °C. After that, the dried NH_2-treated GNDs (30 mg mL^{-1} in water, 3.0 wt % with respect to water) were redispersed into distilled water through the sonochemical treatment for 1 h.

Synthesis of Reduced Graphene Oxide Sheets. RGO was prepared by using modified Hummers and Ruoff methods.[47,48,64] To preoxidize the natural graphite powders, 5 g of graphite powder, 2.5 g of P_2O_5, and 2.5 g of $K_2S_2O_8$ were added into 30 mL of H_2SO_4, then the mixed solution was heated at 90 °C for 6 h. The mixture was washed with excess distilled water through a cellulose acetate filter (Whatmann Inc., USA). The preoxidized powder was dried in a vacuum oven at room temperautre for 1 d. The preoxidized graphites were mixed with 2.5 g of $NaNO_3$ in 120 mL of of H_2SO_4 followed by vigorrous stirring for 30 min in an ice bath. 15.0 g of $KMnO_4$ was slowly added into the solution with temperature lower than 20 °C for 45 min, followed by heat treatment of the solution at 35 °C for 4 h, and the brownish gray paste formed. After addition of 600 mL of distilled water and 25 mL of H_2O_2 solution into the brownish gray paste, the color of paste changed into a bright yellow. The yellowish paste was washed with 5 wt % HCl and distilled water for several times to balance the pH of solution to 7. Then the solution was sonicated to exfoliate graphitic oxide into graphene oxide (GO), followed by centrifuation at 6000 rpm to exclude residues. As-prepared GO (1 mg mL^{-1}, in DMF/water mixture) powder was redispersed into a mixture of DMF/water (95:5, v/v), and the GO was reduced by adding hydrazine monohydrate (1/1000 v/v vs DMF/water) into a DMF/water mixture with vigorous stirring at 95 °C for 1 h. The reduced graphene oxide (RGO) solution was washed with excess distilled water, then dried in a vacuum oven at room temperature for 1 d. Finally, the solid RGO (30 mg mL^{-1} in DMF/water mixture, 2.1 wt % with respect to DMF/water mixture) was dissolved in the mixture of DMF/water (95:5, v/v).

Fabrication of PVDF/NH_2-Treated GND/RGO Nanocomposite. To prepare NH_2-treated GND/RGO cofiller solution, 0.6 mL of

DOI: 10.1021/acsami.5b01430
ACS Appl. Mater. Interfaces 2015, 7, 9668−9681

supernatant solution of NH_2-treated GND was added to 0.6 mL of RGO solution, and the mixture of NH_2-treated GND/RGO was vigorously stirred for 2 h and sonochemically treated for 1 h. Then, 2.5 g of PVDF and 1.2 mL of NH_2-treated GND/RGO cofiller (1:1, v/v) solution was mixed with 10.5 mL of PVDF solution (0.24 g mL^{-1} in DMF) with vigorous stirring at 1000 rpm for 1 d using a magnetic stirrer (C-MAG HS 7, IKA Works, Inc. Germany). Therefore, the vol % of NH_2-treated GND/RGO in the PVDF nanocomposite could be calculated using eq 6:

$$\frac{v_{GND} + v_{RGO}}{v_{GND} + v_{RGO} + v_{PVDF}} \times 100 = \frac{0.6mL + 0.6mL}{10.5mL + 0.6mL + 0.6mL} \times 100 = 10\ vol\% \quad (6)$$

where v_{GND}, v_{RGO}, and v_{PVDF} denote the volume of NH_2-treated GND (0.6 mL, 30 mg mL^{-1} in water, 3.0 wt % with respect to DMF/water mixture), RGO (0.6 mL, 30 mg mL^{-1} in DMF/water mixture, 3.1 wt % with respect to DMF/water mixture), and PVDF (10.5 mL, 0.24 g mL^{-1} in DMF, 25.0 wt % with respect to DMF) solutions, respectively. The wt % of NH_2-treated GND/RGO in the PVDF/NH_2-treated GND/RGO nanocomposite was determined using eq 7:

$$\frac{(v_{GND} \times d_{GND}) + (v_{RGO} \times d_{RGO})}{(v_{GND} \times d_{GND}) + (v_{RGO} \times d_{RGO}) + (v_{PVDF} \times d_{PVDF})} \times 100wt\% = 1.42wt\% \quad (7)$$

where d_{GND}, d_{RGO}, and d_{PVDF} denote the density of NH_2-treated GND (30 mg mL^{-1} in water, 3.0 wt % with respect to water), (RGO 30 mg mL^{-1} in DMF/water mixture, 3.1 wt % with respect to DMF/water mixture), and PVDF solutions (0.24 g mL^{-1} in DMF, 25.0 wt % with respect to DMF), respectively. Furthermore, the content of the PVDF/NH_2-treated/RGO nanocomposites in the mixture solution can be calculated using eq 8:

$$[(v_{GND}d_{GND}) + (v_{RGO}d_{RGO}) + (v_{PVDF}d_{PVDF})] / [(v_{GND}d_{GND}) + (v_{RGO}d_{RGO}) + (v_{PVDF}d_{PVDF}) + (v_{solvent}d_{sovent})] \times 100wt\% = 18.6wt\% \quad (8)$$

where $v_{solvent}$ and $d_{solvent}$ refer to the volume (11.7 mL) and the density (0.95 g mL^{-1}) of the DMF/water (99.7:0.3, v/v) mixture solvent, respectively. In detail, the content of the NH_2-treated GND/RGO cofiller (1:1, v/v), PVDF, and DMF/water mixture solvent were calculated as 2.6, 18.3, and 81.4 wt %, respectively. For the static light-scattering measurement of the nanocomposite, the PVDF/NH_2-treated/RGO nanocomposite solutions with different PVDF/NH_2-treated/RGO contents (1, 2, 5, and 10 wt %) were prepared by adding different amounts of the DMF solvent (12, 30, 120, and 250 mL, respectively) to the 18.6 wt % nanocomposite solution. The mixed solutions were sonochemically treated using an ultrasonicator (VCX 500, Sonics & Materials. Inc. USA) for 1 h to promote the dispersions of the NH_2-treated GNDs and RGO sheets in the PVDF matrix. The sonochemically treated solution was deposited onto a glass substrate using spin-coating method (EC101D, Headway Research, Garland, TX), and the spin-coated glass was dried at room temperature for 1 d. The thickness of nanocomposite was ca. 35 μm.

Isothermal Melt-Crystallization Experiment. POM images were obtained using a Nikon Lv100 microscope (Nikon, Japan) equipped with a custom-designed T-jump cell (CU-109, Live Cell Instruments, Seoul, Korea) containing two silver heating stages for isothermal crystallization. The sample coated on a glass substrate was maintained on a heating stage at 220 °C for 10 min and subsequently moved to another heating stage that provides the desired crystalline temperature. To compare the spherulite growth rates of the samples, the samples on the second heating stage were kept at different temperatures (145, 150, 155, 160, and 165 °C). To observe the γ-phase formation in the samples, the samples on the second heating stage were kept at 160 °C for 24 h after being annealed to 170 or 180 °C. After being annealed, the samples were cooled (30 °C min^{-1}) to room temperature.

Static Light-Scattering Experiment. The static light-scattering experiment of the PVDF/NH_2-treated/RGO nanocomposite solution was conducted using a superstatic light-scattering spectrophotometer (SLS, SLS-6500, Otsuka Electronics Co., Ltd. Japan). The light-scattering intensity $I(q) = I_{solution} - I_{solvent}$ could be measured as a function of scattering vector $q = (4\pi n/\lambda_0)\sin\theta/2$, where the n, λ_0, and θ refer to the refractive reference of DMF (n = 1.427), wavelength of a He−Ne laser (λ_0 = 632.8 nm), and scattering angle, respectively.

Instrumental Analyses. Morphological images of the NH_2-treated GND and RGO were recorded on a transmission electron microscope (TEM, LIBRA 120, Carl Zeiss, Germany). Fourier transform-infrared (FT-IR) spectra were obtained with Frontier FT-IR spectrometers (PerkinElmer Inc. Waltham, MA, USA). X-ray diffractograms (XRDs) were recorded on a Bruker D8 DISCOVER X-ray diffractometer (Bruker, Germany). Differential scanning calorimetry (DSC) data were obtained with a differential scanning calorimeter (Q1000, TA Instruments, Austin, TX) with a heating rate of 10 °C min^{-1} and a cooling rate of 8 °C min^{-1} from 25 to 240 °C under nitrogen atmosphere. Raman spectra were measured on T6 spectrometer (Horiba−Jobin−Yvon Co., Tokyo, Japan). The dielectric properties were measured using a frequency response analyzer (FRA1260, Solartron−Schlumberger, Farnborough, U.K.). The polarization−electric field (P−E) curves and energy densities of the nanocomposites were investigated using a function generator (FG300, Yokogawa, Japan), a digital oscilloscope (DL7100, Yokogawa, Japan), and a voltage amplifier (610E, Trek, USA).

■ ASSOCIATED CONTENT

Ⓢ Supporting Information

Tabulated Hansen solubility parameters, POM image, plot of spherulite growth rate, FT-IR spectra, tabulated IR data, XRD spectra, Hoffman−Weeks plots, tabulated Hoffman−Weeks data. The Supporting Information is available free of charge on the ACS Publications website at DOI: 10.1021/acsami.5b01430.

■ AUTHOR INFORMATION

Corresponding Author

*E-mail: jsjang@plaza.snu.ac.kr.

Notes

The authors declare no competing financial interest.

■ ACKNOWLEDGMENTS

This work was supported by Global Frontier R&D Program on Center for Multiscale Energy System funded by the National Research Foundation under the Ministry of Education, Science and Technology, Korea (2011-0031573).

■ REFERENCES

(1) Greforio, R., Jr.; Cestari, M.; Bernardino, F. E. Dielectric Behaviour of Thin Films of β-PVDF/PZT and β-PVDF/$BaTiO_3$ Composites. *J. Mater. Sci.* **1996**, *31*, 2925−2930.

(2) Lee, B.-S.; Park, B.; Yang, H.-S.; Han, J. W.; Choong, C.; Bae, J.; Lee, K.; Yu, W.-R.; Jeong, U.; Chung, U.-I.; Park, J.-J.; Kim, O. Effects of Substrate on Piezoelectricity of Electrospun Poly(vinylidene fluoride)-Nanofiber-Based Energy Generators. *ACS Appl. Mater. Interfaces* **2014**, *6*, 3520−3527.

(3) Fabiano, S.; Crispin, X.; Berggren, M. Ferroelectric Polarization Induces Electric Double Layer Bistability in Electrolyte-Gated Field-Effect Transistors. *ACS Appl. Mater. Interfaces* **2014**, *6*, 438−442.

(4) Cauda, V.; Stassi, S.; Bejtka, K.; Canavese, G. Nanoconfinement: An Effective Way to Enhance PVDF Piezoelectric Properties. *ACS Appl. Mater. Interfaces* **2013**, *5*, 6430−6437.

(5) Meador, M. A. B.; McMillon, E.; Sandberg, A.; Barrios, E.; Wilmoth, N. G.; Mueller, C. H.; Miranda, F. A. Dielectric and Other

DOI: 10.1021/acsami.5b01430
ACS Appl. Mater. Interfaces 2015, 7, 9668−9681

Properties of Polyimide Aerogels Containing Fluorinated Blocks. *ACS Appl. Mater. Interfaces* **2014**, *6*, 6062−6068.
(6) Schanze, K. S.; Shelton, A. H. Functional Polyelectrolytes. *Langmuir* **2009**, *25*, 13698−13702.
(7) Mendes, F.; Costa, C. M.; Caparros, C.; Sencadas, V.; L-Mendez, S. Effect of Filler Size and Concentration on the Structure and Properties of Poly(vinylidene fluoride)/$BaTiO_3$ Nanocomposites. *J. Mater. Sci.* **2012**, *47*, 1378−1388.
(8) Fabiano, S.; Crispin, X.; Berggren, M. Ferroelectric Polarization Induces Electric Double Layer Bistability in Electrolyte-Gated Field-Effect Transistors. *ACS Appl. Mater. Interfaces* **2014**, *6*, 438−442.
(9) Duan, C.-G.; Mei, W. N.; Yin, W.-G.; Liu, J.; Hardy, J. R.; Ducharme, S.; Dowben, P. A. Simulations of Ferroelectric Polymer Film Polarization: The Role of Dipole Interactions. *Phys. Rev. B* **2004**, *69*, 235106−1−6.
(10) Tiwari, V. K.; Prasad, A. K.; Singh, V.; Jana, K. K.; Misra, M.; Prasad, C. D.; Maiti, P. Nanoparticle and Process Induced Super Toughened Piezoelectric Hybrid Materials: The Effect of Stretching on Filled System. *Macromolecules* **2013**, *46*, 5595−5603.
(11) Kang, S. J.; Park, Y. J.; Bae, I.; Kim, K. J.; Kim, H.-C.; Bauer, S.; Thomas, E. L.; Park, C. Printable Ferroelectric PVDF/PMMA Blend Films with Ultralow Roughness for Low Voltage Non-Volatile Polymer Memory. *Adv. Funct. Mater.* **2009**, *19*, 2812−2818.
(12) Bae, I.; Kim, R. H.; Hwang, S. K.; Kang, S. J.; Park, C. Laser-Induced Nondestructive Patterning of a Thin Ferroelectric Polymer Film with Controlled Crystals Using $Ge_8Sb_2Te_{11}$ Alloy Layer for Nonvolatile Memory. *ACS Appl. Mater. Interfaces* **2014**, *6*, 15171−15178.
(13) Park, Y. J.; Kang, S. J.; Shin, Y.; Kim, R. H.; Bae, I.; Park, C. Non-Volatile Memory Characteristics of Epitaxially Grown PVDF-TrFE Thin Films and Their Printed Micropattern Application. *Curr. Appl. Phys.* **2011**, *11*, e30−e34.
(14) Shin, Y. J.; Kang, S. J.; Jung, H. J.; Park, Y. J.; Bae, I.; Choi, D. H.; Park, C. Chemically cross-linked thin poly(vinylidene fluoride-cotrifluoroethylene) films for nonvolatile ferroelectric polymer memory. *ACS Appl. Mater. Interfaces* **2011**, *3*, 582−589.
(15) Sharma, T.; Je, S.-S.; Gill, B.; Zhang, J. X. J. Patterning Piezoelectric Thin Film PVDF−TrFE based Pressure Sensor for Catheter Application. *Sens. Actuators, A* **2012**, *177*, 87−92.
(16) Electromechanical Characterization of Piezoelectric PVDF Polymer Films for Tactile Sensors in Robotics Applications. *Sens. Actuators, A* **2011**, *169*, 49−58;.
(17) Martins, P.; Caparros, C.; Gonçalves, R.; Martins, P. M.; Benelmekki, M.; Botelho, G.; Lanceros-Mendez, S. Role of Nanoparticle Surface Charge on The Nucleation of The Electroactive β-Poly(vinylidene fluoride) Nanocomposites for Sensor and Actuator Applications. *J. Phys. Chem. C* **2012**, *116*, 15790−15794.
(18) Merlini, C.; Barra, G. M. O.; Araujo, T. M.; Pegoretti, A. Electrically Pressure Sensitive Poly(vinylidene fluoride)/Polypyrrole electrospun mats. *RSC Adv.* **2014**, *4*, 15749−15758.
(19) Zhang, D.; Pickering, K.; Gabbitas, B.; Cao, P.; Langdon, A.; Torrens, R.; Verbeek, J. Actuation Behavior of CP Actuator Based on Polypyrrole and PVDF. *Adv. Mater. Res.* **2007**, *29*, 363−366.
(20) Zhang, P.; Zhao, X.; Zhang, X.; Lai, Y.; Wang, X.; Li, J.; Wei, G.; Su, Z. Electrospun Doping of Carbon nanotubes and Platinum Nanoparticles into The β-phase Polyvinylidene Difluoride Nanofibrous Membrane for Biosensor and Catalysis Applications. *ACS Appl. Mater. Interfaces* **2014**, *6*, 7563−7571.
(21) Lee, J. S.; Shin, K.-Y.; Kim, C.; Jang, J. Enhanced Frequency Response of a Highly Transparent PVDF−Graphene-based Thin Film Acoustic Actuator. *Chem. Commun.* **2013**, *49*, 11047−11049.
(22) Kim, P.; Doss, N. M.; Tillotson, J. P.; Hotchikiss, P. J.; Pan, M.-J.; Marder, S. R.; Li, J.; Calame, J. P.; Perry, J. W. High Energy Density Nanocomposites Based on Surface-Modified $BaTiO_3$ and a Ferroelectric Polymer. *ACS Nano* **2009**, *3*, 2581−2592.
(23) Zhou, T.; Zha, J.-W.; Cui, R.-Y.; Fan, B.-H.; Yuan, J.-K.; Dang, Z.-M. Improving Dielectric Properties of $BaTiO_3$/Ferroelectric Polymer Composites by Employing Surface Hydroxylated $BaTiO_3$ Nanoparticles. *ACS Appl. Mater. Interfaces* **2011**, *3*, 2184−2188.
(24) Li, J.; Claude, J.; N-Franco, L. E.; Seok, S. I.; Wang, Q. Electrical Energy Storage in Ferroelectric Polymer Nanocomposites Containing Surface-Functionalized $BaTiO_3$ Nanoparticles. *Chem. Mater.* **2008**, *20*, 6304−6306.
(25) Liu, S.; Zhai, J.; Wang, J.; Xue, S.; Zhang, W. Enhanced Energy Storage Density in Poly(vinylidene fluoride) Nanocomposites by a Small Loading of Suface-Hydroxylated $Ba_{0.6}Sr_{0.4}TiO_3$ Nanofibers. *ACS Appl. Mater. Interfaces* **2014**, *6*, 1533−1540.
(26) Tang, H.; Zhou, Z.; Sodano, H. A. Relationship Between $BaTiO_3$ Nanowire Aspect Ratio and The Dielectric Permittivity of Nanocomposites. *ACS Appl. Mater. Interfaces* **2014**, *6*, 5450−5455.
(27) Fonseca, C. P.; Benedetti, J. E. Neves, Improving The Dielectric Constant and Energy Density of Poly(vinylidene fluoride) Composites Induced by Surface-Modified $SrTiO_3$ Nanofibers by Polyvinylpyrrolidone. *J. Mater. Chem. A* **2015**, *3*, 1511−1517.
(28) Fonseca, C. P.; Benedetti, J. E.; Neves, S. Poly(3-methyl thiophene)/PVDF Composite As an Electrode for Supercapacitors. *J. Power Sources* **2006**, *158*, 789−794.
(29) Shehzad, K.; Ul-Haq, A.; Ahmad, S.; Mumtaz, M.; Hussain, T.; Mujahid, A.; Shah, A. T.; Choudhry, M. Y.; Khokhar, I.; Ul-Hassan, S.; Nawaz, F.; ur Rahman, F.; Butt, Y.; Pervaiz, M. All-Organic PANI−DBSA/PVDF Dielectric Composites With Unique Electrical Properties. *J. Mater. Sci.* **2013**, *48*, 3737−3744.
(30) Park, T.; Kim, B.; Kim, Y.; Kim, E. Highly conductive PEDOT electrodes for harvesting dynamic energy through piezoelectric conversion. *J. Mater. Chem. A* **2014**, *2*, 5462−5469.
(31) Sharma, M.; Madras, G.; Bose, S. Cooperativity and Structural Relaxations in PVDF/PMMA Blends in The Presence of MWNTs: an Assessment through SAXS and Dielectric Spectroscopy. *Macromolecules* **2014**, *47*, 1392−1402.
(32) Ahn, Y.; Lim, J. Y.; Hong, S. M.; Lee, J.; Ha, J.; Choi, H. J.; Seo, Y. Enhanced Piezoelectric Properties of Electrospun Poly(vinylidene fluoride)/Multiwalled Carbon Nanotube Composites due to High β-phase Formation in Poly(vinylidene fluoride). *J. Phys. Chem. C* **2013**, *117*, 11791−11799.
(33) Rahman, Md. A.; Lee, B.-C.; Phan, D.-T.; Chung, G.-S. Fabrication and Characterization of Highly Efficient Flexible Energy Harvesters Using PVDF−Graphene Nanocomposites. *Smart Mater. Struct.* **2013**, *22*, 085017.
(34) Rahman, A. Md.; Chung, G.-S. Synthesis of PVDF-Graphene Nanocomposites and Their Properties. *J. Alloys Compd.* **2013**, *581*, 724−730.
(35) Andrew, J. S.; Clarke, D. R. Enhanced Ferroelectric Phase Content of Polyvinylidene Difluoride Fibers with The Addition of Magnetic Nanoparticles. *Langmuir* **2008**, *24*, 8435−8438.
(36) Sencadas, V.; Martins, P.; Pitaes, A.; Benelmekki, M.; Gomez Ribelles, J. L.; Lanceros-Mendez, S. Influence of Ferrite Nanoparticle Type and Content on The Crystallization Kinetics and Electroactive Phase Nucleation of Poly(vinylidene fluoride). *Langmuir* **2011**, *27*, 7241−7249.
(37) Wang, D.; Bao, Y.; Zha, J.-W.; Zhao, J.; Dang, Z.-M.; Hu, G.-H. Improved Dielectric Properties of Nanocomposites Based on Poly(vinylidene fluoride) and Poly(vinyl alcohol)-Functionalized Graphene. *ACS Appl. Mater. Interfaces* **2012**, *4*, 6273−6279.
(38) Wen, F.; Xu, Z.; Tan, S.; Xia, W.; Wei, X.; Zhang, Z. Chemical Bonding-Induced Low Dielectric Loss and Low Conductivity in High-*k* Poly(vinylidenefluoride-trifluorethylene)/Graphene Nanosheets Nanocomposites. *ACS Appl. Mater. Interfaces* **2013**, *5*, 9411−9420.
(39) Shang, J.; Zhang, Y.; Yua, L.; Shen, B.; Lv, F.; Chu, P. K. Fabrication and Dielectric Properties of Oriented Polyvinylidene Fluoride Nanocomposites Incorporated with Graphene Nanosheets. *Mater. Chem. Phys.* **2012**, *134*, 867−874.
(40) Li, R.; Chen, C.; Li, J.; Xu, L.; Xiao, G.; Yan, D. A Facile Approach to Superhydrophobic and Superoleophilic Graphene/Polymer Aerogels. *J. Mater. Chem. A* **2014**, *2*, 3057−3064.
(41) Achaby, M. E.; Arrakhiz, F. Z.; Vaudreuila, S.; Essassi, E. M.; Qaiss, A. Piezoelectric β-Polymorph Formation and Properties Enhancement in Graphene Oxide−PVDF Nanocomposite Films. *Appl. Surf. Sci.* **2012**, *258*, 7668−7677.

DOI: 10.1021/acsami.5b01430
ACS Appl. Mater. Interfaces 2015, 7, 9668−9681

(42) Yang, X. J.; Li, J. Y.; Lei, Y. P. The Preparation and Dielectric Properties of BT/PANI/PVDF Composite. *Adv. Mater. Res.* **2013**, *668*, 17−20.
(43) Yao, S.−H.; Dang, Z.−M.; Jiang, M.−J.; Bai, J. $BaTiO_3$-Carbon Nanotube/Polyvinylidene Fluoride Three-Phase Composites with High Dielectric Constant and Low Dielectric Loss. *Appl. Phys. Lett.* **2008**, *93*, 182905−1−3.
(44) Li, Y.; Huang, X.; Hu, Z.; Jiang, P.; Li, S.; Tanaka, T. Large Dielectric Constant and High Thermal Conductivity in Poly(vinylidene fluoride)/Barium Titanate/Silicon Carbide Three-Phase Nanocomposites. *ACS Appl. Mater. Interfaces* **2011**, *3*, 4396−4403.
(45) Liu, H.; Shen, Y.; Song, Y.; Nan, C.−W.; Lin, Y.; Yang, X. Carbon Nanotube Array/Polymer Core/Shell Structured Composites with High Dielectric Permittivity, Low Dielectric Loss, and Large Energy Density. *Adv. Mater.* **2011**, *23*, 5104−5108.
(46) Shang, J.; Zhang, Y.; Yu, L.; Luan, X.; Shen, B.; Zhang, Z.; Lv, F.; Chu, P. K. Fabrication and Enhanced Dielectric Properties of Graphene−Polyvinylidene Fluoride Functional Hybrid Films with a Polyaniline Interlayer. *J. Mater. Chem. A* **2013**, *1*, 884−890.
(47) Stankovich, S.; Dikin, D. A.; Piner, R. D.; Kohlhaas, K. A.; Kleinhammes, A.; Jia, Y.; Wu, Y.; Nguyen, S. T.; Ruoff, R. S. Synthesis of Graphene-Based Nanosheets via Chemical Reduction of Exfoliated Graphite Oxide. *Carbon* **2007**, *45*, 1558−1565.
(48) Long, D.; Hong, J.-Y.; Li, W.; Miyawaki, J.; Ling, L.; Mochida, I.; Yoon, S.-H.; Jang, J. Fabrication of Uniform Graphene Discs via Transversal Cutting of Carbon Nanofibers. *ACS Nano* **2011**, *5*, 6254−6261.
(49) Lee, E.; Ryu, J.; Jang, J. Fabrication of Graphene Quantum Dots via Size-Selective Precipitation and Their Application in Upconversion-Based DSSCs. *Chem. Commun.* **2013**, *49*, 9995−9997.
(50) Chen, L.; Guo, C. X.; Zhang, Q.; Lei, Y.; Xie, J.; Ee, S.; Guai, G.; Song, Q.; Li, C. M. Graphene Quantum-Dot-Doped Polypyrrole Counter Electrode for High-Performance Dye-Sensitized Solar Cells. *ACS Appl. Mater. Interfaces* **2013**, *5*, 2047−2052.
(51) Peng, J.; Gao, W.; Gupta, B. K.; Liu, Z.; Romero-Aburto, R.; Ge, L.; Song, L.; Alemany, L. B.; Zhan, X.; Gao, G.; Vithayathil, S. A.; Kaipparettu, B. A.; Marti, A. A.; Hayashi, T.; Zhu, J. J.; Ajayan, P. M. Graphene Quantum Dots Derived from Carbon Fibers. *Nano Lett.* **2012**, *12*, 844−849.
(52) Yan, X.; Cui, X.; Li, L.-S. Synthesis of Large, Stable Colloidal Graphene Quantum Dots with Tunable size. *J. Am. Chem. Soc.* **2010**, *132*, 5944−5945.
(53) Liu, Y.; Wu, P. Graphene Quantum Dot Hybrids as Efficient Metal-Free Electrocatalyst for The Oxygen Reduction Reaction. *ACS Appl. Mater. Interfaces* **2013**, *5*, 3362−3369.
(54) Huang, Z.; Shen, Y.; Li, Y.; Zheng, W.; Xue, Y.; Qin, C.; Zhang, B.; Hao, J.; Feng, W. Facile Synthesis of Analogous Graphene Quantum Dots with sp^2 Hybridized Carbon Atom Dominant Structures and Their Photovoltaic Application. *Nanoscale* **2014**, *6*, 13043−13052.
(55) Routh, P.; Das, S.; Shit, A.; Bairi, P.; Das, P.; Nandi, A. K. Graphene Quantum Dots from a Facile Sono-Fenton Reaction and Its Hybrid with a Polythiophene Graft Copolymer Toward Photovoltaic Application. *ACS Appl. Mater. Interfaces* **2013**, *5*, 12672−12680.
(56) Zhang, M.; Bai, L.; Shang, W.; Xie, W.; Ma, H.; Fu, Y.; Fang, D.; Sun, H.; Fan, L.; Han, M.; Liu, C.; Yang, S. Facile Synthesis of Water-Soluble, Highly Fluorescent Graphene Quantum Dots as a Robust Biological Label for Stem Cells. *J. Mater. Chem.* **2012**, *22*, 7461−7467.
(57) Dong, Y.; Tian, W.; Ren, S.; Dai, R.; Chi, Y.; Chen, G. Graphene Quantum Dots/L-Cysteine Coreactant Electrochemiluminescence System and Its Application in Sensing Lead(II) Ions. *ACS Appl. Mater. Interfaces* **2014**, *6*, 1646−1651.
(58) Shen, J.; Zhu, Y.; Yang, X.; Zong, J.; Zhang, J.; Li, C. One-Pot Hydrothermal Synthesis of Graphene Quantum Dots Surface-Passivated By Polyethylene Glycol and Their Photoelectric Conversion under Near-Infrared Light. *New J. Chem.* **2012**, *36*, 97−101.
(59) Wang, X.; Sun, X.; Lao, J.; He, H.; Cheng, T.; Wang, M.; Wang, S.; Huang, F. Multifunctional Graphene Quantum Dots for Simultaneous Targeted Cellular Imaging and Drug Delivery. *Colloids Surf., B* **2014**, *122*, 638−644.
(60) Zhou, Z.-J.; Liu, Z.-B.; Li, Z.-R.; Huang, X.-R.; Sun, C.-C. Shape Effect of Graphene Quantum Dots on Enhancing Second-Order Nonlinear Optical Response and Spin Multiplicity in NH_2−GQD−NO_2 Systems. *J. Phys. Chem. C* **2011**, *115*, 16282−16286.
(61) Jiang, F.; Chen, D.; Li, R.; Wang, Y.; Zhang, G.; Li, S.; Zheng, J.; Huang, N.; Gu, Y.; Wang, C.; Shu, C. Eco-Friendly Synthesis of Size-Controllable Amine-Functionalized Graphene Quantum Dots with Antimycoplasma Properties. *Nanoscale* **2013**, *5*, 1137−1142.
(62) Fei, H.; Ye, R.; Ye, G.; Gong, Y.; Peng, Z.; Fan, X.; Samuel, E. L. G.; Ajayan, P. M.; Tour, J. M. Boron- and Nitrogen-Doped Graphene Quantum Dots/Graphene Hybrid Nanoplatelets as Efficient Electrocatalysts for Oxygen Reduction. *ACS Nano* **2014**, *8*, 10837−10843.
(63) Hansen, C. M. *Hansen Solubility Parameters: A User's Handbook,* 2nd ed.; CRC Press: Hoboken, NJ, 2007.
(64) Park, S.; An, J.; Jung, I.; Piner, R. D.; An, S. J.; Li, X.; Velamakanni, A.; Ruoff, R. S. Colloidal Suspensions of Highly Reduced Graphene Oxide in a Wide Variety of Organic Solvents. *Nano Lett.* **2009**, *9*, 1593−1597.
(65) Pham, V. H.; Cuong, T. V.; Hur, S. H.; Oh, E.; Kim, E. J.; Shin, E. W.; Chung, J. S. Chemical Functionalization of Graphene Sheets by Solvothermal Reduction of a Graphene Oxide Suspension in *N*-Methyl-2-Pyrrolidone. *J. Mater. Chem.* **2011**, *21*, 3371−3377.
(66) Gong, F.; Xu, X.; Zhou, G.; Wang, Z.-S. Enhanced Charge Transportation in a Polypyrrole Counter Electrode via Incorporation of Reduced Graphene Oxide Sheets for Dye-Sensitized Solar Cells. *Phys. Chem. Chem. Phys.* **2013**, *15*, 546−552.
(67) Elzayat, M. Y. F.; El-Sayed, S.; Osman, H. M.; Amin, M. X-ray Diffraction and Differential Scanning Calorimetry Studies of a $BaTiO_3$/Polyvinylidene Fluoride Composites. *Polym. Eng. Sci.* **2012**, *52*, 1945−1950.
(68) Sun, L.-L.; Li, B.; Zhao, Y.; Zhong, W.-H. Suppression of AC Conductivity by Crystalline Transformation in Poly(vinylidene fluoride)/Carbon Nanofiber Composites. *Polymer* **2010**, *51*, 3230−3237.
(69) Bhimasankaram, T.; Suryanarayana, S. V.; Prasad, G. Piezoelectric Polymer Composite Materials. *Curr. Sci.* **1998**, *74*, 967−976.
(70) Furukawa, T.; Ishida, K.; Fukuda, E. Piezoelectric Properties in The Composite Systems of Polymers and PZT Ceramics. *J. Appl. Phys.* **1979**, *50*, 4904−4913.
(71) Hu, J.; Zhang, J.; Fu, Z.; Jiang, Y.; Ding, S.; Zhu, G. Solvent Vapor Annealing of Ferroelectric P(VDF-TrFE) Thin Films. *ACS Appl. Mater. Interfaces* **2014**, *6*, 18312−18318.
(72) Shin, Y. J.; Kim, R. H.; Jung, H. J.; Kang, S. J.; Park, Y. J.; Bae, I.; Park, C. Compression of Cross-Linked Poly(vinylidene fluoride-co-trifluoroethylene) Films for Facile Ferroelectric Polarization. *ACS Appl. Mater. Interfaces* **2011**, *3*, 4736−4743.
(73) Chang, D. W.; Lee, E. K.; Park, E. Y.; Yu, H.; Choi, H.-J.; Jeon, I.-Y.; Sohn, G.-J.; Shin, D.; Park, N.; Oh, J. H.; Dai, L.; Baek, J.-B. Nitrogen-Doped Graphene Nanoplatelets from Simple Solution Edge-Functionalization for n-Type Field-Effect Transistors. *J. Am. Chem. Soc.* **2013**, *135*, 8981−8988.
(74) Kavitha, T.; Kang, I.-K.; Park, S.-Y. Poly(acrylic acid)-Grafted Graphene Oxide as an Intracellular Protein Carrier. *Langmuir* **2014**, *30*, 402−409.
(75) Ha, H. W.; Choudhury, A.; Kamal, T.; Kim, D.-H.; Park, S.-Y. Effect of Chemical Modification of Graphene on Mechanical, Electrical, and Thermal Properties of Polyimide/Graphene Nanocomposites. *ACS Appl. Mater. Interfaces* **2012**, *4*, 4623−4630.
(76) Socrates, G. *Infrared and Raman Characteristic Group Frequencies: Tables and Charts,* 3rd ed.; Wiley-VCH: Weinheim, Germany, 1993.
(77) Lanceros-Méndez, S.; Mano, J. F.; Costa, A. M.; Schmidt, V. H. FTIR and DSC Studies of Mechanically Deformed β-PVDF Films. *J. Macromol. Sci., Part B: Phys.* **2001**, *B40*, 517−527.
(78) Mondal, T.; Bhowmick, A. K.; Krishnamoorti, R. Stress Generation and Tailoring of Electronic Properties of Expanded

DOI: 10.1021/acsami.5b01430
ACS Appl. Mater. Interfaces 2015, 7, 9668−9681

Graphite by Click Chemistry. *ACS Appl. Mater. Interfaces* **2014**, *6*, 7244−7253.
(79) Yang, Q. H.; Hou, P. X.; Unno, M.; Yamauchi, S.; Saito, R.; Kyotani, T. Dual Raman Features of Double Coaxial Carbon Nanotubes with N-Doped and B-Doped Multiwalls. *Nano Lett.* **2005**, *5*, 2465−2469.
(80) Wei, D.; Liu, Y.; Wang, Y.; Zhang, H.; Huang, L.; Yu, G. Synthesis of N-Doped Graphene by Chemical Vapor Deposition and Its Electrical Properties. *Nano Lett.* **2009**, *9*, 1752−1758.
(81) Hoffman, J. D.; Weeks, J. J. Melting Process and the Equilibrium Melting Temperature of Polychlorotrifluoroethylene. *J. Res. Natl. Bur. Stand.* **1962**, *66*, 13−28.
(82) Abolhasani, Md. M.; Naebe, M.; Jalali-Arani, A.; Guo, Q. Influence of Miscibility Phenomenon on Crystalline Polymorph Transition in Poly(vinylidene fluoride)/Acrylic Rubber/Clay Nanocomposite Hybrid. *PLoS One* **2014**, *9*, e88715−1−8.
(83) Gregorio, R., JR.; Capitao, R. C. Morphology and Phase Transition of High Melt Temperature Crystallized Poly(vinylidene fluoride). *J. Mater. Sci.* **2000**, *35*, 299−266.
(84) Gregorio, R., JR. Determination of the α, β, and γ Crystalline Phases of Poly(vinylidene fluoride) Films Prepared at Different Conditions. *J. Appl. Polym. Sci.* **2006**, *100*, 3272−3279.
(85) Prest, W. M.; Luca, D. J. The morphology and thermal response of high−temperature−crystallized poly(vinylidene fluoride). *J. Appl. Phys.* **1975**, *46*, 4136−4143.
(86) Higgins, J. S.; Benoit, H. C. *Polymers and Neutron Scattering;* Clarendon Press: Oxford, U.K., 1994.
(87) Fuller, G. G. *Optical Rheometry of Complex Fluids: Theory and Practice of Optical Rheometry;* Oxford University Press: Oxford, U.K., 1995.
(88) Sarazin, D.; Picot, C.; Patlazhan, S. Structure of Poly(vinylidene difluoride) Solutions in Acetone. *Macromolecules* **2006**, *39*, 1226−1233.

DOI: 10.1021/acsami.5b01430
ACS Appl. Mater. Interfaces 2015, 7, 9668−9681